Neuron, Vol. 23, 181–192, May, 1999, Copyright ©1999 by Cell Press

A YAC Mouse Model for Huntington's Disease with Full-Length Mutant Huntingtin, Cytoplasmic Toxicity, and Selective Striatal Neurodegeneration

J. Graeme Hodgson,[1] Nadia Agopyan,[3] Claire-Anne Gutekunst,[5] Blair R. Leavitt,[1] Fred LePiane,[2] Roshni Singaraja,[1] Desmond J. Smith,[6] Nagat Bissada,[1] Krista McCutcheon,[1] Jamal Nasir,[1] Laure Jamot,[4] Xiao-Jiang Li,[5] Mary E. Stevens,[6] Erica Rosemond,[3] John C. Roder,[4] Anthony G. Phillips,[2] Edward M. Rubin,[6] Steven M. Hersch,[5] and Michael R. Hayden[1,7]

[1]Centre for Molecular Medicine and Therapeutics
University of British Columbia
Vancouver, British Columbia V5Z 4H4

[2]Department of Psychology
University of British Columbia
Vancouver, British Columbia V6T 1Z4

[3]Faculty of Pharmacy
University of Toronto
Toronto, Ontario L4V 1V7

[4]Department of Molecular Immunology and Neurobiology
University of Toronto
Toronto, Ontario M5G 1X5
Canada

[5]Emory University School of Medicine
Atlanta, Georgia 30322

[6]Human Genome Center
Lawrence Berkeley Laboratories
Berkeley, California 94720

Summary

We have produced yeast artificial chromosome (YAC) transgenic mice expressing normal (YAC18) and mutant (YAC46 and YAC72) huntingtin (htt) in a developmental and tissue-specific manner identical to that observed in Huntington's disease (HD). YAC46 and YAC72 mice show early electrophysiological abnormalities, indicating cytoplasmic dysfunction prior to observed nuclear inclusions or neurodegeneration. By 12 months of age, YAC72 mice have a selective degeneration of medium spiny neurons in the lateral striatum associated with the translocation of N-terminal htt fragments to the nucleus. Neurodegeneration can be present in the absence of macro- or microaggregates, clearly showing that aggregates are not essential to initiation of neuronal death. These mice demonstrate that initial neuronal cytoplasmic toxicity is followed by cleavage of htt, nuclear translocation of htt N-terminal fragments, and selective neurodegeneration.

Introduction

Huntington's disease (HD) is characterized by personality change, involuntary movements, and dementia typically beginning in midadulthood and progressing toward death ~18 years from onset (Hayden, 1981; Harper, 1991). The hallmark neuropathological feature of HD is neuronal loss in the caudate and putamen (Vonsattel et al., 1985), primarily affecting the medium spiny projection neurons. The underlying genetic defect is expansion to >35 of a CAG trinucleotide repeat in the *HD* gene (Huntington's Disease Collaborative Research Group, 1993).

Recent studies have implicated the formation of aggregates containing truncated polyglutamine-containing fragments in the pathogenesis of CAG trinucleotide diseases (Davies et al., 1997). Immunohistochemical analyses have demonstrated the presence of neuronal, intranuclear inclusions in postmortem material from HD (DiFiglia et al., 1997), spinocerebellar ataxia (SCA) 1 (Skinner et al., 1997), SCA3 (Paulson et al., 1997), and dentatorubral pallidoluysian atrophy (DRPLA) (Becher et al., 1997) patients and in mice expressing exon 1 of huntingtin (htt). Despite the observed association of aggregates with neurodegeneration, the relationship between aggregation and cell death remains unresolved (Klement et al., 1998; Saudou et al., 1998).

Our goal was to generate transgenic mice that replicate, within the context of the full-length *HD* gene, the disease-causing genetic mutation, expressed in the same developmental and tissue- and cell-specific manner seen in patients with the disease. To this end, yeast artificial chromosomes (YACs) containing human genomic DNA spanning the full-length gene, including all regulatory elements, were used. The HD clones were engineered to contain CAG sizes similar to those seen in either adult onset (YAC46 containing 46 CAG repeats) or juvenile onset (YAC72 containing 72 CAG repeats) HD.

We found that YAC46 and YAC72 mice develop progressive electrophysiological abnormalities that precede nuclear translocation and aggregation of htt. YAC72 mice have behavioral abnormalities, with onset influenced by the level of mutant protein. A mouse expressing mutant htt with 72 glutamines at higher levels presented with an early onset behavioral phenotype (~6 weeks) and had intranuclear aggregates and neurodegeneration specifically in the striatum. Other YAC72 mice expressing lower levels of mutant protein had progressive electrophysiologic abnormalities at 6 and 10 months, followed by selective striatal neurodegeneration first seen at 12 months of age. No aggregates were visible by light or electron microscopy, clearly indicating that aggregates are not necessary for initiation of selective neuronal loss. On the other hand, translocation of N-terminal fragments of htt into the nucleus is seen, providing in vivo evidence of cleavage of htt and the toxic gain of function of these fragments, as first proposed by Goldberg et al. (1996). These mice represent the first animal model expressing full-length mutant human htt under the control of its own promoter, providing insights into the sequential molecular and cellular events underlying HD.

[7]To whom correspondence should be addressed (e-mail: mrh@cmmt.ubc.ca).

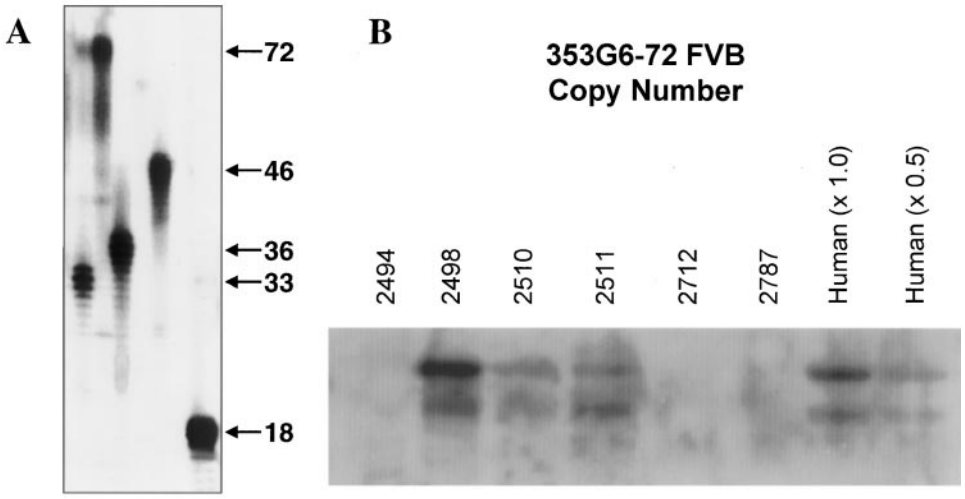

Figure 1. Generation of 46 and 72 CAGs in YACs

(A) Homologous recombination was used to introduce 46 and 72 CAG repeats into YACs containing 18 CAG repeats.

(B) Southern blot of YAC72 transgenic founder mice using human HD–specific probe cD70–2. The copy number in founder F2498 is higher than that of two other full-length founders (2510 and 2511) and human DNA. Founders 2494, 2712, and 2787 are missing this portion of the YAC. Equal amounts (10 μg) of DNA were loaded per lane.

Results

YAC Transgenic Mice

Two well-characterized YACs (YGA2 and 353G6) containing 18 CAG repeats and spanning the entire *HD* gene (Hodgson et al., 1996) were used.

We adopted a previously described strategy using homologous recombination in yeast to introduce expanded CAG repeats (46 and 72) into YACs (Duff et al., 1994) (Figure 1A). Since YACs are inherently unstable, and this strategy relies on homologous recombination, all clones were extensively screened by Southern analysis, PCR, and pulse-field gel electrophoresis.

Southern analysis comparing signal intensity with human genomic DNA demonstrated that all YAC46 transgenic lines had integrated one to two copies of the YAC (data not shown). Two of the seven lines injected with YAC72 integrated the complete *HD* gene (2498 and 2511). Densitometric scanning showed that founder 2498 had integrated approximately four copies of the transgene (two wild-type), whereas line 2511 integrated one to two copies (Figure 1B). We were able to establish lines from all founder mice with the exceptions of YAC46 664 and YAC72 2498, which developed an early neurological phenotype at 6 weeks of age (see below) and did not breed.

Transgene-Derived htt Is Expressed in a Pattern Similar to Endogenous htt

Both normal and mutant human htt were expressed in the same tissues as the endogenous mouse protein, with highest levels seen in brain and testes (Figure 2A). Subcellular localization experiments on cortical tissue from wild-type and transgenic mice showed that mutant YAC-derived htt primarily localized to the cytosolic and membrane-associated fractions (data not shown), similar to human htt (DiFiglia et al., 1995).

Additionally, in light of the observed electrophysiological changes in the hippocampi of YAC46 and YAC72 mice (see below), we confirmed that human htt was expressed in the hippocampi of YAC transgenic mice by Western blot (Figure 2B) and by immunohistochemistry (data not shown). Expression was low in peripheral tissues, similar to humans.

Mutant htt expression in fibroblast cell lines revealed htt expression in YAC72 founder 2498 to be approximately three times that seen in founder 2511 (Figure 2C) and approximately twice that of endogenous levels (data not shown). Expression levels in YAC18, YAC46, and YAC72 (2511) lines were equivalent, representing one-third to one-half of endogenous level expression (Figure 2D).

Rescue of Embryonic Lethality

We next tested for appropriate developmental regulation by assessing whether mice expressing mutant human htt (YAC46 or YAC72) could compensate for the loss of endogenous htt. Targeted disruption of htt results in embryonic lethality at 7.5 days gestation (Duyao et al., 1995; Nasir et al., 1995; Zeitlin et al., 1995). We crossed the YAC46 and YAC72 lines onto the null background and demonstrated efficient rescue of the embryonic lethality. The genotype of the YAC-positive offspring at the mouse HD locus had the expected Mendelian 1:2:1 ratio for homozygous, heterozygous, and wild-type offspring (35:68:26, respectively). In contrast, cDNA transgenic mice expressing full-length htt with 18, 44, and 128 glutamines under the control of the cytomegalovirus promoter failed to rescue the embryo lethality.

These data provide conclusive evidence of appropriate developmental expression of mutant htt under the control of the endogenous promoter and show that expansion of the polyglutamine tract does not disrupt normal function of htt in mammalian development.

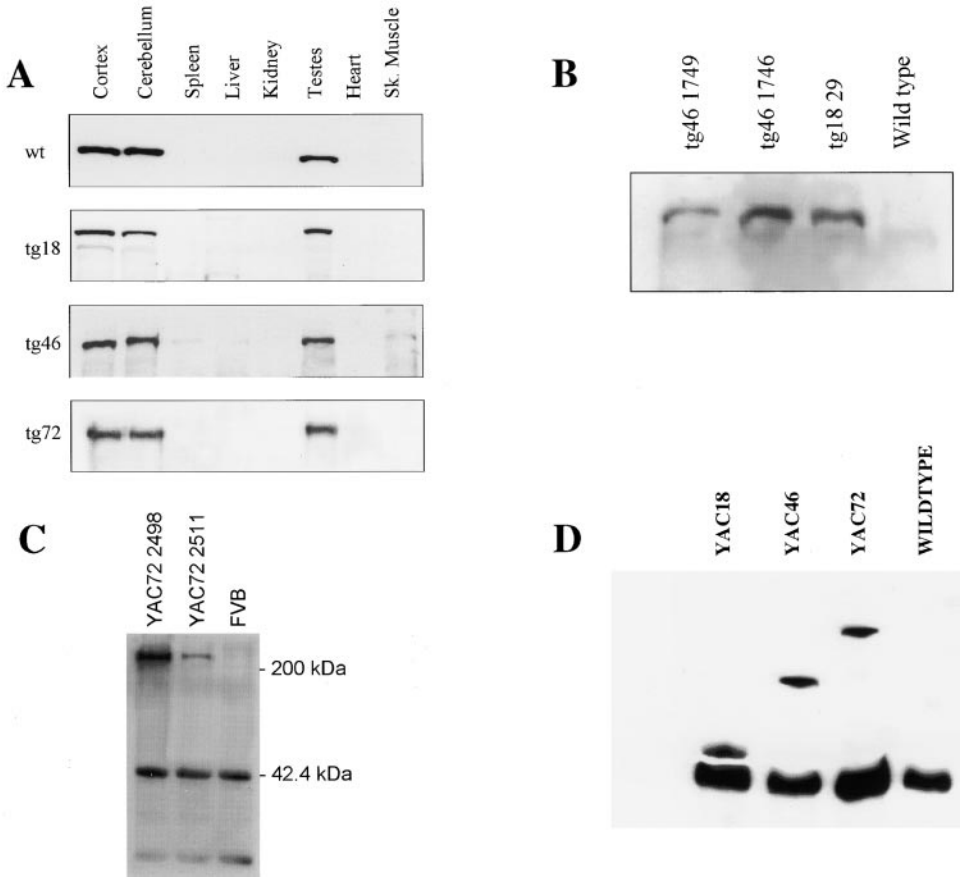

Figure 2. Human htt Expression in YAC Transgenic Mice Parallels that Seen with Endogenous Mouse htt Expression

(A) The tissue expression patterns of wild-type (wt) and human htt in YAC18 (tg 18), YAC46 (tg 46), and YAC72 (tg 72) mice. Normal and YAC transgenic proteins (100 μg of total protein from each tissue) were probed with BKP1 (detects murine and human htt) and GHM1 (detects human htt only). Htt expression levels are highest in cortex, cerebellum, and testes. A longer exposure of the blots indicated murine and human htt are also expressed at low levels in other tissues tested.

(B) Western blot using human-specific monoclonal antibody GHM1 showing hippocampal expression of human htt in two YAC46 (1749 and 1746) and YAC18 (line 29) mice.

(C) YAC transgenic mice expressing human htt with 72 glutamines have varying levels of expression, depending on the copy number of the gene. YAC72 founder 2498 expresses human htt at higher levels than founder 2511 using lysates from fibroblast lines assessed using GHMI. Equal loading was confirmed by equivalent actin levels in each lane.

(D) YAC18, YAC46, and YAC72 transgenic mice express human htt at equivalent levels that are approximately one-third to one-half of endogenous htt expression.

Motor and Behavioral Analysis

Tests were designed to detect behavioral and motor deficits in wild-type (n = 7), YAC18 (line 30, n = 7), and YAC46 (line 668, n = 7; line 1747, n = 3) mice. Tests were repeated at 2 month intervals between 3 and 20 months of age. In addition, observations were made on the YAC72 mice lines and age-matched controls at 3, 5, 7, and 9 months of age. All mice used in this study were pure FVB/N, eliminating the confounding effects of strain differences. YAC18 mice behaved identically to wild-type mice at all ages tested.

YAC46

Weekly observation of mouse behavior and handling of the mice revealed no obvious differences in behavior compared with wild-type or YAC18 mice up to 20 months of age. Responsiveness to sensory stimuli, including auditory cues, olfactory cues, and touch; spontaneous activity measurements; motor control; and coordination were normal.

YAC72

The weight of the YAC72 mouse (2498) was approximately half that of her female siblings (16 g versus 29.9 g; n = 3) when sacrificed at 1 year. YAC72 mice from line 2511 had body weight similar to controls at all times assessed.

Observations of spontaneous behavior were carried out on the 2498 mouse (Figure 3A) and age-matched controls (Figure 3B) at the ages of 3, 5, 7, and 9 months. The 2498 mouse showed obvious circling that was persistent and by 9 months was associated with obvious choreoathetoid movements of the head and neck as well as gait ataxia. The circling was tight and rapid, with a full turn being completed in approximately one-third of a second (Figure 3C). When held by the tail, 2498 was disoriented and displayed a foot-clasping posture reminiscent of HD exon 1 transgenic mice (Mangiarini et al., 1996). Additionally, as it was lowered to the bench top, unlike wild-type FVB/N mice, it failed to orient itself

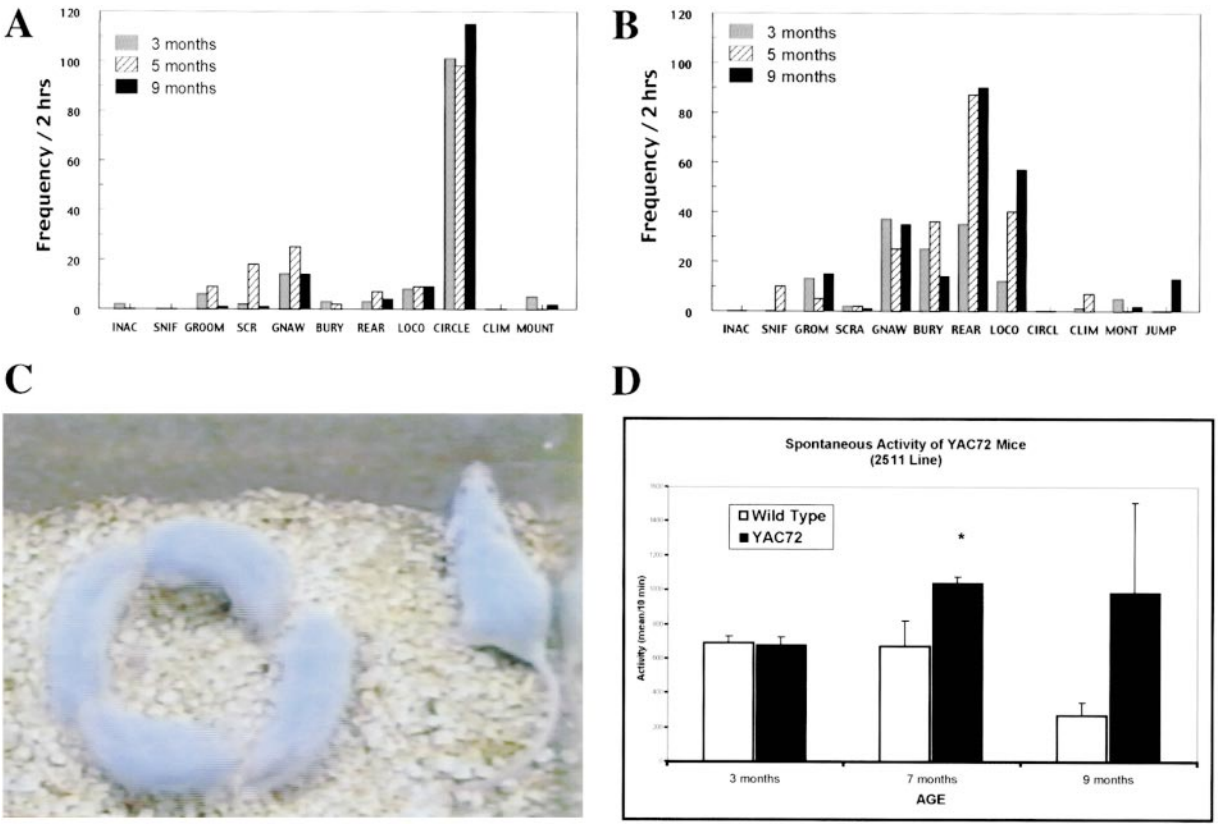

Figure 3. Motor and Behavioral Phenotypes of YAC72 Mice

Behavioral profile of YAC72 mouse 2498 (A) and nontransgenic control mice (B) at 3, 5, and 9 months of age. Tight, rapid circling was the predominant behavior in founder 2498.

(C) Composite image derived from video footage of mouse 2498's circling behavior. The time taken to complete the circle is approximately one-third of a second. YAC72 mice (line 2511) develop a late onset circling behavior at 9 months, similar to the 2498 founder. A nontransgenic age-matched control is shown in the top right-hand corner.

(D) Spontaneous activity measures for wild-type and YAC72 (line 2511) mice tested as independent groups at 3, 7, and 9 months of age. YAC72 mice show hyperactivity compared with wild-type at 7 and 9 months of age but not at 3 months. Data are expressed as mean activity over 10 min during dark phase ± SEM. Mean activity was significantly different from that of wild type at $p < 0.03$ (asterisk) using the Student's t test.

upright. In addition, it failed to successfully complete the beam-crossing task.

Mice from the low-expressing YAC72 line (2511) did not manifest with any obvious behavioral phenotype until 7 months of age. These mice display a mild hyperkinetic movement disorder characterized by progressive spontaneous hyperactivity during the dark phase of open field testing ($p < 0.03$) (Figure 3D). In one mouse, stereotypical unidirectional circling developed at 8.5 months, similar to behavior seen at an earlier age in the high-expressing YAC72 mouse (Figure 3C). At 9 months, differences in activity during the dark phase were again seen in YAC72 mice (Figure 3D). Even though as a group, the mutant mice were more hyperactive compared with wild-type, there was considerable variability in this result because of the extreme hyperactivity of one mouse with circling behavior. Excluding this mouse from the mutant group still revealed the significance of the hyperactivity ($p < 0.05$) of the YAC72 mice compared with wild-type.

Electrophysiology

Since hippocampal neuronal loss occurs frequently in HD (Spargo et al., 1993), and mutant htt is expressed in the hippocampus in YAC transgenic mice and humans (Gutekunst et al., 1995) (Figure 2B), we examined the effect of CAG expansion on synaptic transmission and plasticity prior to development of a behavioral phenotype. We compared the induction and maintenance of homosynaptic long-term potentiation (LTP) at the Schaeffer collateral–CA1 synapses of the hippocampus in control, YAC46, and YAC72 mice.

To standardize slices from different groups, we elicited synaptic responses at an intensity that was 50% of that required to induce a population spike and measured differences in saturated LTP achieved by repeating tetanic stimulation five times.

At 6 months, maintenance of LTP at 60 min was 127% ± 5% for YAC46 mice (line 668, $n = 8$), 170% ± 12% for YAC46 mice (line 1747, $n = 4$), 221% ± 107% for YAC72 mice (line 2511, $n = 4$), 179% ± 20% for YAC18 mice ($n = 8$), and 183% ± 30% for wild-type ($n = 10$) (not significant) (Figure 4A1). Slices from 6-month-old mice with 72 CAG repeats displayed hyperexcitability, which manifested itself as epileptiform activity at the somatic level, and a very broad excitatory postsynaptic potential (EPSP) at the distal dendrites

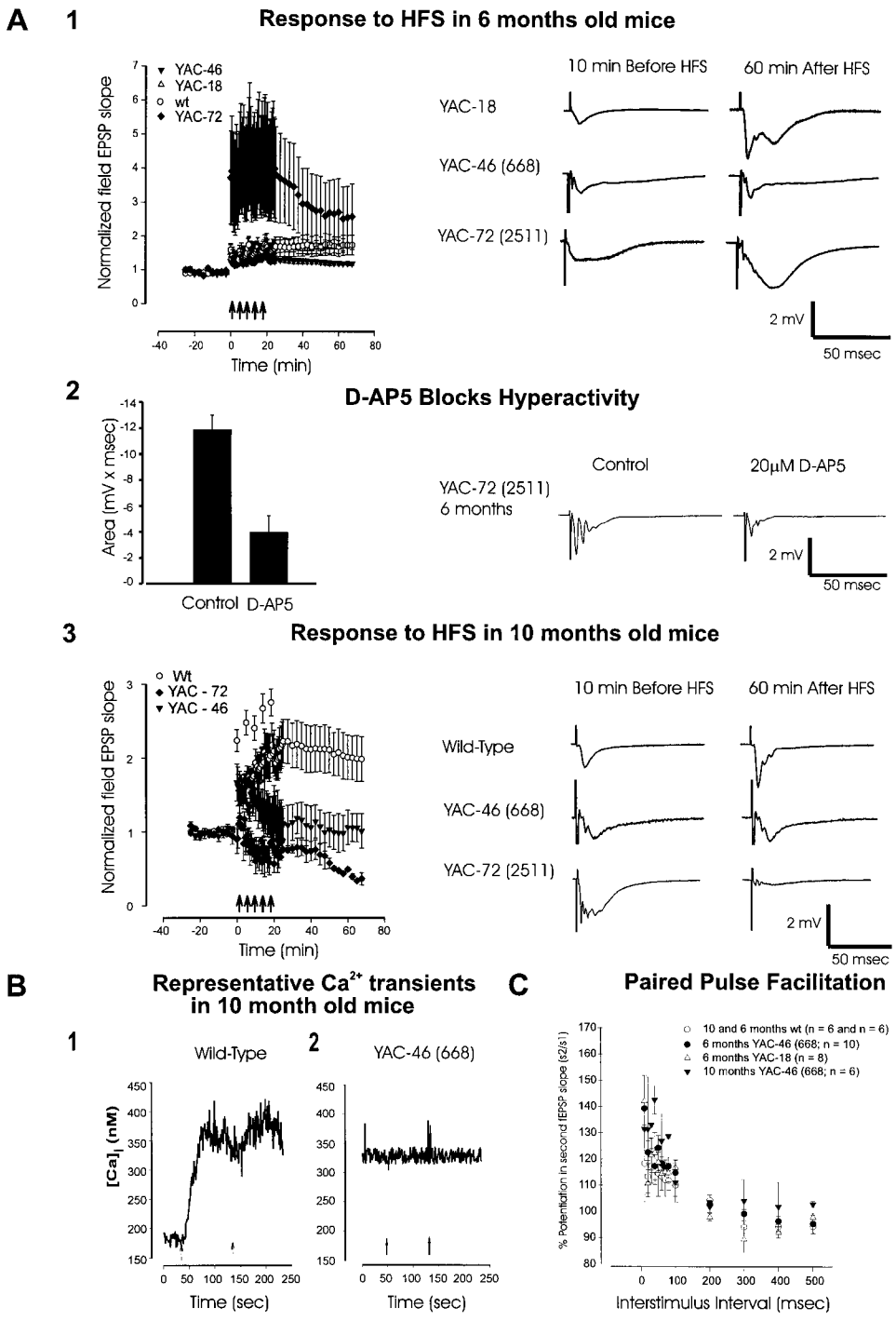

Figure 4. Effect of CAG Expansion on Synaptic Transmission

Graphs in (A1) and (A3) summarize LTP obtained from 6- and 10-month wild-type (wt), YAC18, YAC46, and YAC72 (line 2511) mice, respectively. Data are plotted as the mean fEPSP slope ± SEM (normalized with respect to the 10 min immediately preceding the tetanus) versus time. Each point is an average of ten traces within 5 min bins. The baseline stimulation intensity was 30%–50% of the maximal response delivered every 30 s and was constant. Arrows indicate the time at which individual HFS was delivered. The traces are representative field recordings (averages of ten sweeps) showing the responses 10 min before (baseline) and 60 min after HFS. In (A2), D-AP5 blocks the hyperactivity seen in the dendritic region of 6-month-old YAC72 (2511) mice. The bar histograms show the area under the fEPSP in the absence and presence of D-AP5 (25 μM).

(B) Elevated resting calcium levels and lack of calcium influx in response to glutamate in 10-month-old YAC46 mice. Intracellular resting calcium concentrations are increased in CA1 pyramidal neurons from YAC46 mice (B) (335 ± 70 [n = 6]) compared with wild-type mice (A) (165 ± 12 [n = 6] [$p < 0.05$]). Neurons from 10 month YAC46 (line 668) mice did not respond to either 10 mM or 100 mM glutamate (arrows) in contrast to wild-type mice.

(C) PPF is not altered in YAC46 mice compared with wild-type mice at 6 and 10 months of age.

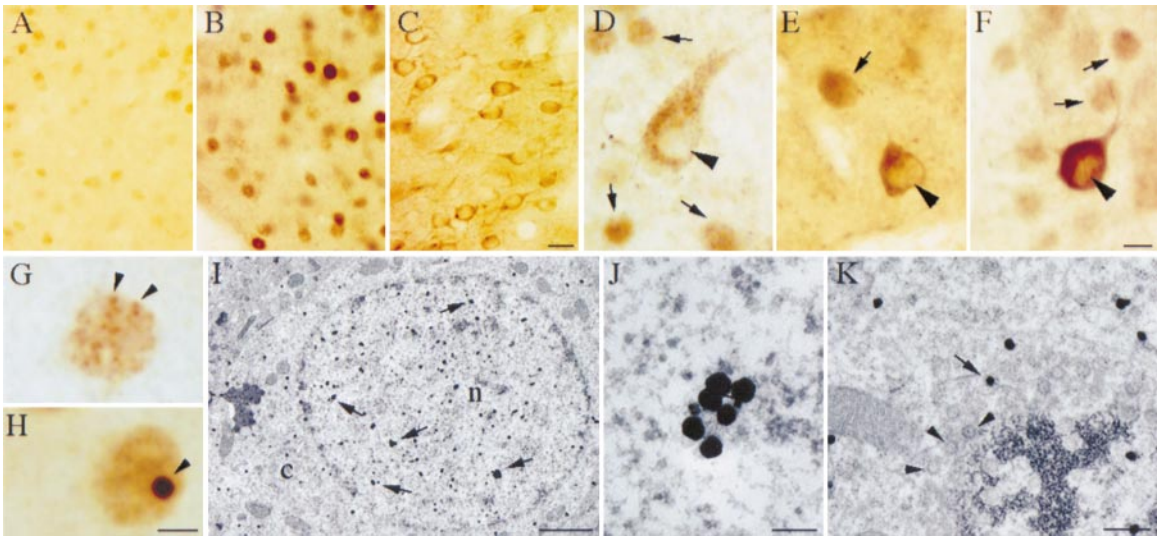

Figure 5. N-Terminal htt Aggregates in the YAC72 2498 Mouse

(A) and (B) are light micrographs showing EM48 immunoreactivity in the striatum of a wild-type control and mouse 2498, respectively. EM48 immunoreactivity is obviously more intense in the nuclei of the striatal mouse 2498 than in wild type. EM48 immunoreactivity was very intense in neuronal nuclei (B), whereas HD549 immmunoreactivity was restricted to the cytoplasm (C). EM48 nuclear immunoreactivity (arrow) did not occur in VAT- (D), NOSI- (E), or PARV- (F) immunoreactive neurons (arrowheads). Nuclear staining was diffuse and also included small (G) and large ([H], arrowheads) puncta. By electron microscopy (I), immunogold particles were seen both in the cytoplasm (c) and nucleus (n). Microaggregates containing more than five particles were found in the nuclei ([I], arrows). At higher magnification, microaggregates appear to be associated with amorphous, electron-dense material (J). Particles were also found in nuclear pores ([K], arrows). Nuclear pores not containing immunogold particles are indicated by the arrowheads (K). Scale bar, 30 μm (A–C); 10 μm (D–F); 8 μm (G and H); 3 μm (I); 50 nm (J); and 100 nm (K).

(Figure 4A1). 2-amino-5-phosphonovalerate (D-AP5) (25 uM), which blocks NMDA receptors (Morris et al., 1986) and under normal conditions has no effect on the fast synaptic response, blocked the somatic spiking and reduced the area under the field EPSP (fEPSP) curve (Figure 4A2; -11.75 ± 0.189 mV.ms in control slices ($n = 4$) and -3.82 ± 0.24 mV.ms in D-AP5-treated slices ($n = 4$) in 6-month-old YAC72 mice. These findings suggest that in 6-month-old YAC72 mice, the NMDA component is prominent during fast synaptic transmission. Following tetanization, most of the slices from YAC72 mice displayed a greater short-term potentiation (372% ± 124%, $p = 0.20$ when compared with wild-type and YAC18), which progressively declined over time.

By 10 months of age, obvious and significant differences were seen in both YAC46 and YAC72 mice. In contrast to wild-type, LTP was not induced in CA1 neurons of either line of mice expressing mutant htt (Figure 4A3). The potentiation at 60 min after the fifth tetanus in slices from 10 month YAC46 mice was 101% ± 25% (line 668, $n = 6$) and 108% ± 12% (line 1746, $n = 6$) compared with 199% ± 31% ($n = 6$) in wild-type mice ($p < 0.01$). High-frequency stimulation (HFS) induced depression instead of potentiation in 10 month YAC72 mice (Figure 4A3). Lack of LTP induction in mutant slices was not due to the deterioration of slices, as no change in the responses within the same slice from the nontetanized control pathway was recorded.

To determine the mechanism underlying the progressive loss of LTP in 10 month YAC46 mice, we next investigated whether glutamate-mediated calcium influx, which is a crucial factor in the induction of LTP (Malenka et al., 1988, 1992), was intact in these mice. Calcium transients in Fura-2-loaded, acutely dissociated hippocampal CA1 neurons from 10-month-old YAC46 mice consistently failed to produce a calcium signal in response to glutamate application (Figure 4B) in contrast to controls.

Lack of calcium influx can result from downregulation of NMDA receptors and/or reduced driving force for calcium. In keeping with these possibilities, resting levels of calcium in neurons from these mutant mice were higher (335 ± 70 nM [$n = 6$]) than those of controls (165 ± 12 nM [$n = 6$] [$p < 0.05$]) (Figure 4B), suggesting that the calcium-buffering capacity of mutant neurons was reduced.

Elevated intracellular calcium concentration can also affect presynaptic release mechanisms. To assess presynaptic efficacy, we investigated the extent of the paired-pulse facilitation (PPF) in wild-type, YAC18, and YAC46 mice, which showed no differences from controls at 6 and 10 months of age (Figure 4C).

However, posttetanic potentiation, which is the potentiation seen immediately after tetanic stimulation and is also indicative of presynaptic release mechanisms, was reduced in 10-month-old YAC46 mice. The normalized fEPSP slope immediately after the first HFS was 224% ± 15% in wild-type mice ($n = 6$), 167% ± 25% in Transgenic line 668 ($n = 5$), and 102% ± 9% in transgenic line 1746 ($n = 6$) ($p < 0.05$). These data suggest that presynaptic terminals in mutant mice, while responding normally to single stimuli, are not able to sustain neurotransmitter release during high-frequency stimulation.

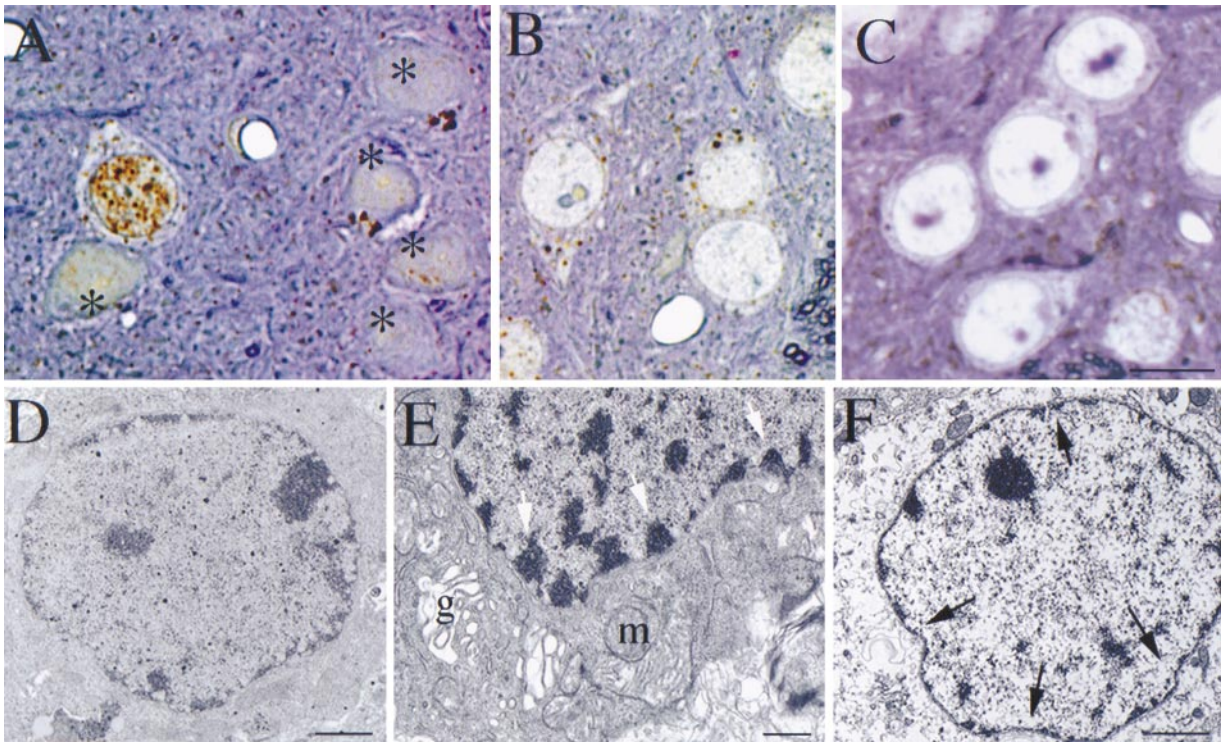

Figure 6. Neurodegeneration in Mouse 2498

(A) through (C) are micrographs of 1.5 μm striatal sections from YAC72 2498 (A and B) and YAC18 (C) immunoreacted with EM48 and counterstained with toluidine blue. In YAC72 2498, many degenerating neurons (stars) are present in the most lateral regions of the striatum ([A], stars) as compared with the more medial regions (B). In YAC18, neurons had a normal appearance, with a regular and well-rounded nuclear envelope (C). Intense EM48 staining (brown) is seen in a neuronal nucleus (A) in the lateral striatum and in the cytoplasm of neurons in the medial portion of the striatum (B). Many degenerated neurons contained immunogold particles in their nuclei (n) and cytoplasm (c). In (D), evidence of degeneration included condensed cytoplasm, swelling of mitochondria (m), vacuolation of Golgi (g), and condensation and marginization of the heterochromatin ([E], arrows). By electron microscopy, many neurons that did not show frank degenerative signs had abnormal scalloped nuclear membranes (F). Scale bar, 20 μm (A–C); 3 μm (D); 200 nm (E); and 3 μm (F).

Neuropathology: Nuclear Translocation of N-Terminal htt

Brains from wild-type (n = 7), YAC18 (n = 4), and YAC46 (n = 5) mice were examined at 5, 9, 12, and 20 months of age. The brains of YAC72 mice were examined only at 5 (n = 2), 8 (n = 2), 10 (n = 3), and 12 ([n = 3] [2511], [n = 1] [2498]) months. The gross morphology of each brain appeared normal, and a reduction in brain weight was observed only in YAC72 mouse 2498 (0.41 versus 0.58 g in controls [n = 3]).

In all mice examined, faint EM48 staining was present in neurons throughout the brain. In contrast, in the 12-month-old YAC72 mouse (2498), EM48 intensely stained many nuclei within neurons in the striatum (Figure 5B), olfactory tubercle, nucleus accumbens, and fundus striati. Small numbers of neurons in the septum and the granule cell layer of the cerebellar cortex also had nuclear EM48 immunoreactivity. This intense nuclear staining was not seen in any other brain regions, including hippocampus, thalamus, and brain stem, nor was it present in YAC18 or YAC46 or in wild-type controls (Figure 5A). EM48 nuclear staining was more intense in the lateral compared with the medial striatum.

In the 12-month-old YAC72 line 2511 (n = 3), there was an increased number of EM48-immunoreactive neuronal nuclei in the striatum (Figure 7A) and cortex (Figure 7B). We and others have proposed that mutant htt is cleaved in the cytoplasm and that only the N-terminal portion of the protein is translocated into the nuclei, where it may form aggregates (Goldberg et al., 1996; Cooper et al., 1998; Hackam et al., 1998; Martindale et al., 1998; Wellington et al., 1998). We also performed immunocytochemistry in adjacent sections using EM48 and HD549, a rat monoclonal antibody that reacts with an internal region of htt (amino acids 549–679). Sections stained with HD549 alone exhibited intense staining of neuronal perikarya and dendrites as described previously (Gutekunst et al., 1995). HD549 immunoreactivity was not detected in neuronal nuclei (Figure 5C), suggesting that only N-terminal fragments of mutant htt (<549 amino acids) translocate to the nuclei.

Nuclear Staining Is Specific to Medium Spiny Neurons

We performed double immunolabeling using EM48 and antibodies specific for each interneuron population, including the vesicular acetylcholine transporter (VAT), which labels cholinergic interneurons; nitric oxide synthese (NOSI), which labels neurons containing somatostatin; neuropeptide Y and reduced nicotinamide adenine dinucleotide phosphate– (NADPH-) diaphorase; and parvalbumin (PARV), which labels a distinct population of

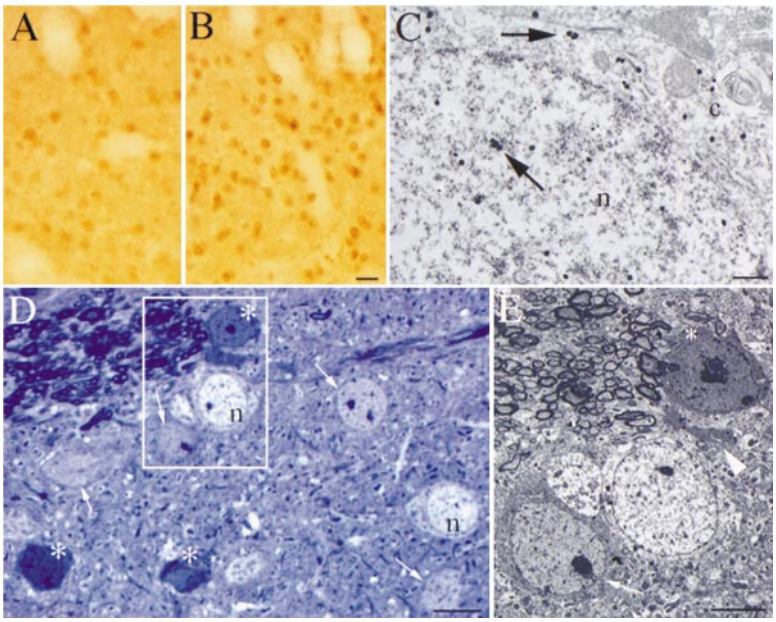

Figure 7. EM48 Immunoreactivity and Neurodegeneration in the 2511 Line

(A) and (B) are micrographs of representative striatal sections from a 1-year-old wild-type control (A) and an age-matched YAC72 mouse from line 2511 (B) stained with EM48. As compared with the wild-type control, many more neuronal nuclei were EM48 positive in the striatum of the YAC72 2511 line. (C) is an electron micrograph showing a striatal neuron containg many EM48 immunogold particles in the nucleus (n), and to a lesser extent, in the cytoplasm (c). Particles were found singly or in clusters of no more than three particles (arrows). (D) is a light micrograph of a representative toluidine blue–stained 1.5 μm semithin section from the lateral portion of the striatum of a YAC72 2511 mouse. Many shrunken and hyperchromatic degenerating neurons are present (stars). In addition, neurons with abnormal morphological changes, including hyperchromasia, can also be seen (arrows) adjacent to normal neurons (n). (E) is an electron micrograph showing the morphological features of the normal, the abnormal (arrow), and the neurodegenerated (star) neurons shown in (D) (inset). A degenerating dendrite can also be seen in the neuropil (arrow). Scale bar, 60 μm (A and B); 350 nm (C); 20 μm (D); and 10 μm (E).

medium-sized interneurons. None of these interneuron populations had nuclear staining by EM48 (Figures 5D–5F), indicating that in the YAC72 striatum, translocation of the N-terminal portion of htt to the nucleus selectively occurs in medium spiny neurons.

Identification of Micro- and Macroaggregates

In YAC72 mouse 2498, many striatal nuclei were diffusely labeled with EM48 and also contained intensely labeled puncta (Figure 5G) that were 1–2 μm in diameter. In the accumbens, some labeled nuclei also contained one or two larger labeled puncta (Figure 5H) that ranged from 2–5 μm and were found in both intensely and lightly stained nuclei. In all stained nuclei, there was a nonstained region corresponding to the nucleoli by electron microscopy. Similar results were obtained using another N-terminal anti-htt antibody raised against the first 17 amino acids of human htt (a gift from Peter Detloff). We have termed these puncta macroaggregates, since they are large enough to be resolved by light microscopy.

To examine potential htt aggregates, we performed immunogold electron microscopy using EM48 on sections containing striatum from YAC72 (2498 and 2511), YAC18, and FVB/N wild-type mice at 12 months of age. In YAC72 mouse 2498, immunogold particles were abundant in the nuclei but were also evident at lower frequency in the cytoplasm (Figure 5I). Within nuclei, immunogold particles were found singly or in clusters (Figures 5I and 5J). Individual immunogold particles could also be identified within nuclear pores (Figure 5K). Most immunogold particles were present singly or in groups of two or three. Larger collections of immunogold particles (>5) were visualized in the nucleus but not in the cytoplasm (Figure 5I). Almost all of these were too small to have been visualized by light microscopy and were thus termed microaggregates. With the same immunogold method and the HD549 antibody, which does not recognize N terminus aggregates, such clusters of immunogold particles have not been seen. These data show that cleavage of htt occurs in the cytoplasm and that N-terminal fragments are translocated through nuclear pores to the nucleus, where they are present in a small number of macroaggregates visible by light microscopy or are diffused through the nucleoplasm as microaggregates visible only by electron microscopy.

In the control and low-expressing YAC72 2511 line mice, immunogold particles were seen in both the cytoplasm and nuclei of neurons. Particles were found mostly singly or in clusters of no more than three particles (Figure 7C). Clusters of more than three particles were only rarely seen in both nucleus and cytoplasm. No macroaggregates were seen by light microscopy, and microaggregates were rare.

Neurodegeneration

Neuronal degeneration was assessed by light microscopy in 1.5 μm thick toluidine blue–stained sections from the striatum, the cortex adjacent to the lateral striatum, the hippocampus, and the cerebellum. YAC18 ($n = 5$); YAC46 ($n = 10$) at 9, 12, and 20 months of age; YAC72 line 2511 at 8 ($n = 4$) and 12 ($n = 3$) months; and the YAC72 2498 mouse at 12 months of age were examined. Degenerating neurons, only present in the striatum, were hyperchromatic and shrunken (Figures 6A and 7D). Unlike striatal neurons, which normally have round nuclei and rounded cellular outlines, degenerating neurons had oval or fusiform perikarya and nuclei. The chromatin within degenerating neurons was also condensed and marginated. Some neurons had morphologic abnormalities that were not severe enough to be considered evidence of cell death but manifested mild hyperchromasia and a more oval cellular shape (Figure 7D).

Electron microscopy using the same tissue blocks confirmed the degenerative and abnormal nature of these morphologic changes. By electron microscopy, degenerative changes varied in severity and included reduced neuronal size, the presence of nuclear and plasma membrane irregularities, increased electron density of the cytoplasm and the nucleus, swelling of some mitochondria, dilation of Golgi cisternae, nuclear shrinkage and condensation, and margination of heterochromatin (Figures 6D, 6E, and 7E). These degenerative features are consistent with apoptosis. In addition to frank degeneration, electron microscopy also revealed frequent irregular nuclear envelopes in neurons (Figure 6F).

Significant degeneration was present in the striatum of the YAC72 2498 mouse and in the YAC72 2511 line at 12 months. No degeneration was found in the YAC46 or YAC18 (Figure 6C) or in wild-type controls. In the striatum of mouse 2498, there was extensive neuronal degeneration, most severe laterally, decreasing in a graded fashion more medially (Figures 6A and 6B). The proportion of degenerating neurons ranged from 4% of observable neurons medially to 80% of neurons laterally. In the striatum of 12-month-old low-expressing YAC72 mice (2511), numerous degenerating neurons (Figure 7D) were present. As in 2498, degenerating neurons were most frequent in the lateral striatum. The medial-to-lateral gradient of neurodegeneration was less dramatic than in the 2498 mouse, ranging from 4% medially to $\sim$40% laterally. We found no sign of degeneration in the YAC72 2511 line at 8 months of age. There was no evidence of reactive gliosis in these mice by glial fibrillary acidic protein immunocytochemistry (data not shown).

The hippocampus was examined, since YAC transgenic mice had abnormal hippocampal LTP, and neuronal loss in the CA1 region of the hippocampus is seen in most patients with HD (Spargo et al., 1993). Examination of semithin and Nissl-stained sections (50 μm) from wild-type, YAC18, and YAC46 mice at ages 5, 9, 12, and 20 months showed no obvious differences in the gross organization and neuronal density of the CA1 pyramidal cell layer and no increase in the presence of degenerating neurons.

Discussion

We have produced YAC transgenic mice that express normal and mutant htt in a developmentally regulated and cell-specific pattern identical to that of endogenous htt and develop functional, behavioral, and pathological changes similar to those of patients with HD. This is manifest with selective neurodegeneration affecting specifically the medium spiny neurons of the striatum. Furthermore, we show that neurodegeneration can occur in the absence of aggregates, providing evidence that aggregates are not essential for the initiation of the illness.

YAC transgenic mice expressing mutant htt with 46 CAG repeats do not have a clinical phenotype by detailed behavioral analysis for up to 20 months of age. However, electrophysiological abnormalities are evident much earlier. The severity of electrophysiological abnormalities is more obvious in mice with 72 compared with 46 CAG repeats at the same age. Interestingly, at 6 months, YAC72 mice had an initial increase in the NMDA component of synaptic response, which was antagonized by D-AP5, an NMDA receptor antagonist. This is consistent with the NMDA receptor hyperactivity associated with the presence of mutant htt. In animals, overactivation of NMDA receptors in the striatum has been shown to reproduce biochemical and neuropathological changes seen in HD (Ferrante et al., 1985; Beal et al., 1989). Recent in vitro data also reveal that mutant htt increases the size of currents through the NMDA receptor subtypes, which are preferentially expressed in the medium spiny neostriatal neurons (Chen et al., 1999). These data represent in vivo evidence in favor of NMDA receptor hyperactivity as an early abnormality in the pathogenesis of HD, consistent with the hypothesis of excitotoxicity in HD (Albin and Greenamyre, 1992; Coyle and Puttfarchen, 1993).

An increase in NMDA receptor function would give rise to an elevated influx of calcium during normal synaptic transmission. Our studies indicated higher resting levels of calcium in neurons from mutant mice at 10 months of age. Increases in intracellular calcium levels are associated with calcium-dependent desensitization of both voltage- and ligand-gated channels, including NMDA receptors. It is therefore possible that during high-frequency stimulation, NMDA receptors are inactivated due to high-calcium influx, which could underlie the lack of LTP in those mice with mutant htt. In both YAC46 and YAC72 mice, the electrophysiological abnormalities precede any obvious behavioral abnormalities as well as any evidence of neurodegeneration or aggregate formation. Taken together, these results suggest that expression of mutant htt in these mice causes cytoplasmic dysfunction before the observed behavioral and neuropathologic changes.

Examination of N terminus htt fragment aggregation in the YAC72 2498 and YAC72 2511 lines does not support the hypothesis that large nuclear aggregates underlie neurodegeneration. In the YAC72 2498 mouse, which expressed high levels of mutant htt and had an obvious behavioral phenotype by 6 weeks of age, 80% of the neurons still observable in the lateral striatum at 1 year of age were undergoing neurodegeneration. In both degenerating and normal-appearing neurons, N-terminal nuclear htt fragments were labeled with solitary and small clusters of immunogold particles, and only rarely were macroaggregates observed. Furthermore, the complete absence of macroaggregates and the rarity of microaggregates in the normal and degenerating striatal neurons in the YAC72 2511 line at 12 months of age suggest that even microaggregates may not be necessary for cell death. The immunogold method, however, does not permit distinguishing solitary N terminus fragments from the smallest possible multimers.

In vitro evidence has suggested that proteolytic cleavage of htt plays an important role in the pathogenesis of htt (Hackam et al., 1998, 1999; Martindale et al., 1998). The studies in the YAC transgenic mice now provide direct evidence of cleavage of htt by demonstration of N-terminal fragments in the nucleus and C-terminal fragments in the cytoplasm. Furthermore, immunogold-labeled electron microscopy has revealed gold-labeled htt fragments traversing the nuclear pore to the nucleus from the cytosol. Importantly, the N-terminal translocation of htt appears to be only evident in those neurons that are

susceptible to subsequent neurodegeneration, namely, the medium spiny neurons. The striatal interneurons, which are largely spared in HD, did not show presence of htt in the nucleus. This suggests that one reason for selective neuronal degeneration in HD might be the generation of proteolytic cleavage of htt in specific cells, with resultant N-terminal translocation of htt into the nucleus specifically in those cells.

The increased intracellular calcium concentration seen in the YAC46 mice at 10 months of age, prior to any evidence of nuclear translocation of htt or apoptosis, supports a model in which the initial trigger for the illness is cytoplasmic toxicity, which is associated with increased cytoplasmic calcium concentration. These findings are highly reminiscent of the recent reports in early onset familial Alzheimer's disease, whereby activation of caspases by mutant presenilin 1 is preceded by an elevation in cytoplasmic calcium (Buxbaum et al., 1998). Altered concentrations of cytoplasmic calcium may be an important trigger for activation of the proteolytic pathways, leading to the generation of truncated fragments for both Alzheimer's disease and HD (Kim and Tanzi, 1998).

Recently, there have been reports of other transgenic mice expressing different portions of htt (Mangiarini et al., 1996; White et al., 1997; Reddy et al., 1998; Schilling et al., 1999) under the control of varying promoters. These mice display a significant neurological phenotype associated with the development of intranuclear aggregates and in some cases, neurodegeneration, but as yet, no evidence of the selective striatal neurodegeneration seen in HD. This suggests that expression of full-length htt and/or expression in a cell-specific and developmental manner, as seen with its own promoter, may be important for accurately recapitulating the disease phenotype.

A major question still left unanswered is, what is the nature of the initial toxic stimulus in the cytoplasm that initiates the cell death pathways, leading to neurodegeneration? One possibility is that there may be disturbed interaction with an interacting protein such as HAP1 (Li et al., 1995) or HIP1 (Kalchman et al., 1997; Wanker et al., 1997), which then induces cellular toxicity and promotes the proteolytic processing of htt.

These YAC transgenic mice represent the first animal model with mutant full-length htt expressed under the control of its endogenous promoter, with all intronic regulatory sequences included. This developmentally appropriate expression of mutant htt in the appropriate cellular compartments has produced animals with behavioral, electrophysiological, and pathological phenotypes occurring at different stages of development, giving insights into the sequence of cellular and molecular events underlying the pathogenesis of HD. In particular, the YAC72 line, with selective striatal neurodegeneration by 1 year of age, allows therapeutic strategies to be assessed that delay or prevent HD.

Experimental Procedures

YAC Mutagenesis

YAC mutagenesis was performed as described previously (Duff et al., 1994). The pop-in construct (see text), containing 46 or 72 CAG repeats, was linearized with BstEII and transformed into yeast spheroplasts. The region of DNA containing the expanded CAG repeat plus sufficient flanking homologous DNA (EE640) was cloned into the pRS406 vector. The EE640 fragment, containing 48 CAG repeats, was cloned from the L191F1 cosmid containing an expanded CAG repeat. This same fragment, containing 72 repeats, was shotgun cloned from patient DNA. These clones were transformed into yeast, and pop-in and pop-out clones were selected as described previously (Duff et al., 1994).

Generation and Screening of YAC Transgenic Mice

YAC DNA was prepared for microinjection into FVB/N pronuclei, and founder pups were screened (Hodgson et al., 1996). Further analysis of the 5′ region of YAC YGA2 was done by Southern analysis using the probes OS14, D4S95, and OT17, a gift from Dr. S. Hadano.

Protein Expression Analysis

Bone marrow fibroblast cultures were established from YAC72 founders 2498 and 2511 and an age-matched FVB/N mouse in Dulbecco's modified Eagle's medium, 10% fetal calf serum, penicillin/streptomycin, and 20 mM L-glutamine (Canadian Life Technologies). Cells were maintained at a humidified atmosphere of 37°C, 6% CO_2. For the isolation of proteins, cells were lysed in buffer (1.0% NP40, 0.15 M NaCl, 50 mM Tris [pH 8.0], and 0.01% azide). Protein (100 μg) was resolved in 7.5% SDS–PAGE minigels. Membranes were reacted with the anti-htt monoclonal antibody GHM1 (Kalchman et al., 1997) or an anti-actin monoclonal antibody (Sigma) by standard conditions.

Behavioral Analysis

Mice were handled and checked on a weekly basis. For a more qualitative assessment, YAC46, YAC18, and control mice were videotaped for 2 hr in a fresh cage identical to the one in which they were housed every 2 months from 8 to 20 months of age. For a 10 s interval every minute, the behavior of the subjects was recorded; the frequency of such behaviors as inactivity, grooming, scratching, sniffing, gnawing, burying, rearing, locomotion, climbing, circling, jumping, and mounting was noted. YAC72 mice (line 2511) were assessed at 3, 7, and 9 months, while YAC72 mouse 2498 was assessed every 2 months from 3 to 12 months of age.

Motor control was tested by the ability to climb a wire screen secured against the wall at a 60° angle and was observed until they reached the top or bottom. For coordination, mice were placed midway on a suspended beam and observed for latency of initiative movement, number of falls, and time to reach safety. Mice were assessed for abnormal righting or posturing by suspension by the tail. Spontaneous motor activity was measured with photo beams in a novel test chamber during 2 hr of light and 2 hr of dark as described previously (Nasir et al., 1995).

Electrophysiology

Hippocampal slices (400 μm thick) from 6- and 10-month-old sex-matched mice were obtained as described previously (Dingledine, 1984) and perfused in an interface chamber at 32°C with oxygenated artificial cerebrospinal fluid (ACSF) containing (in mM): NaCl, 124; KCl, 3.0; KH_2PO_4, 1.25; $CaCl_2$, 4.0; $NAHCO_3$, 26.0; and D-glucose, 10 and 10 μm bicucculline methiodide (GMI; Sigma Chemical). In selected slices, 25 μM D-AP5 (Tocris) was added to the perfusate to block NMDA receptors. To invoke tetanus, LTP consisted of five trains of 100 Hz stimulations lasting 200 ms at an intertrain interval of 10 s. A control pathway, which did not receive pattern stimulation, was also monitored to determine the general state of the slice. Slices that demonstrated either an increase or decrease in the fEPSP slope evoked by the stimulation of the control pathway following HFS of the test pathway were omitted from data analysis.

Data are expressed as mean ± SEM, n = number of animals. Significance was tested by the Student's t test. Experiments were done double blind.

Calcium Measurements

Punched cultures of CA1 neurons were dissociated as described previously (Cohen and Wilkin, 1995). Cells were loaded with 5 μM Fura2-AM (Molecular Probes) by incubating them for 45 min at room temperature in ACSF containing (in mM): NaCl, 140; KCl, 5; $MgCl_2$,

1; $CaCl_2$, 2; and HEPES, 10 (buffered to pH 7.3 with NaOH). Fluorescence measurements were conducted by the use of a PTI D104F series microscope (Nikon Diaphot 200) and a 40× oil immersion objective at room temperature. Cell densities were one to five cells per field. Baseline (30 s) measurements were obtained prior to glutamate (10–100 mM) application. Digitonin (20 μM) was added at the end of the experiment to record background fluorescence. Ratio measurements were converted into estimates of $[Ca^{2+}]_i$ according to the Grynkiewicz equation (Grynkiewicz et al., 1985). K_d, R_{min}, R_{max}, F_b380, and F_i380 values were determined with a calcium calibration kit containing Mg^{2+} (Molecular Probes) and were rechecked every week. Estimated values were K_d, 227 ± 5 nM; R_{min}, 0.44; and R_{max}, 5.7.

Antibodies

Four antibodies against various regions of htt were used: a rabbit polyclonal antibody (EM48) to amino acids 1–256 (Gutekunst et al., 1999), a rabbit polyclonal antibody (HD-N) to the first 17 amino acids of human htt (provided by Peter Detloff), a rat monoclonal antibody (HD549) to amino acids 549–679 (Gutekunst et al., 1995), and a monoclonal antibody (GHMI) directed to the internal region of htt (Hodgson et al., 1996). Other antibodies were directed against the VAT, which labels cholinergic interneurons; NOSI (Chemicon International, Temecula, CA), which labels neurons containing somatostatin, neuropeptide Y, and NADPH-diaphorase activity; and PARV (Sigma, St. Louis, MO), which labels another distinct population of medium-sized interneurons.

Light and Electron Microscopic Immunocytochemistry

Each mouse was anesthetized with sodium pentobarbitol, injected intraperitoneally with 300 IU of heparin, and perfused intracardially with 200 ml of 3% paraformaldehyde and 0.15% glutaraldehyde in 0.1 M phosphate buffer (PB) at pH 7.2. Brains were removed and postfixed overnight in 2% paraformaldehyde. Brains were sectioned in ten series of 40 μm coronal sections with a vibratome (Pelco, Redding, CA), collected in PB, and rinsed in 0.05 M phosphate-buffered saline (PBS [pH 7.2]). Light and electron microscopy immunocytochemistry were performed as described previously (Gutekunst et al., 1995, 1999).

For double immunolabeling experiments, EM48 antibody was combined with either VAT, NOSI, or PARV antibody in the primary incubation. Controls included the omission of primary antisera and single labeling for each antibody.

Assessment of Neurodegeneration

Neurodegeneration was assessed in semithin sections (1.5 μm) from striatum, cortex, hippocampus, and cerebellum in all lines. Sections were cut with a Leica Ultracut S ultramicrotome, counterstained with toluidine blue, differentiated in 95% alcohol, and coverslipped. Neuronal degeneration was quantified as follows: sections were visualized on a Nikon Labophot-2 microscope with a 60× lens equipped with a 1 mm^2 ocular grid. A starting frame was systematically selected so that one side of the ocular grid was touching the most lateral portion of the corpus callosum. From this starting point, counts were made with three 240 μm^2 frames obtained by moving the grid toward the medial portion of the striatum, one grid length at a time. This was repeated in each section. Within each frame, all neurons with visible nuclei were counted and categorized as normal or degenerating. In each counting frame, the top and right frame lines were excluded from analysis.

Acknowledgments

We thank our colleagues in our laboratories for useful comments and discussion, in particular, Dr. Cheryl Wellington, Dr. Abigail Hackam, and Ryan Brinkman. We would also like to thank George Sakellaropoulos, Hong Yi, Courtney Dorn, and James S. Mulroy for their technical assistance. This work was supported by grants from the Medical Research Council of Canada (M. R. H. and B. R. L.), the Canadian Genetic Diseases Network, the Huntington Disease Society of America (M. R. H., C. A. G., and X. J. L.), and the National Institutes of Health (NS35255 to S. H. and C. A. G. and NS36232 to X. J. L.). Dr. Michael Hayden is an established investigator of the British Columbia Children's Hospital.

Received March 8, 1999; revised April 12, 1999.

References

Albin, R.L., and Greenamyre, J.T. (1992). Alternative excitotoxic hypothesis. Neurology *42*, 733–738.

Beal, M.F., Lowall, N.W., Swartz, K.J., Ferrante, R.J., and Martin, J.B. (1989). Differential sparing of somatostain-neuropeptide Y and cholinergic neurons following striatal excitotoxin lesions. Synapse *3*, 38–47.

Becher, M.W., Rubinsztein, D.C., Leggo, J., Wagster, M.V., Stine, O.C., Ranen, N.G., Franz, M.L., Abbott, M.H., Sherr, M., MacMillan, et al. (1997). Dentatorubral and pallidoluysian atrophy (DRPLA). Clinical and neuropathological findings in genetically confirmed North American and European pedigrees. Mov. Disord. *12*, 519–530.

Buxbaum, J.D., Choi, E.K., Luo, Y., Lilliehook, C., Crowley, A.C., Merriam, D.E., and Wasco, W. (1998). Calsenilin: a calcium-binding protein that interacts with the presenilins and regulates the levels of a presenilin fragment. Nat. Med. *4*, 1177–1181.

Chen, N., Luo, T., Wellington, C., Metzler, M., McCutcheon, K., Hayden, M.R., and Raymond, L.A. (1999). Subtype-specific enhancement of NMDA receptor currents by mutant huntingtin. J. Neurochem. *72*, 1820–1898.

Cohen, J., and Wilkin, G.P. (1995). Neural Cell Culture (New York: Oxford University Press).

Cooper, J.K., Schilling, G., Peters, M.F., Herring, W.J., Sharp, A.H., Kaminsky, Z., Masone, J., Khan, F.A., Delanoy, M., Borchelt, D.R., et al. (1998). Truncated N-terminal fragments of huntingtin with expanded glutamine repeats form nuclear and cytoplasmic aggregates in cell culture. Hum. Mol. Genet. *7*, 783–790.

Coyle, J.T., and Puttfarchen, P. (1993). Oxidative stress, glutamate, and neurodegenerative diseases. Ann. Neurol. *38*, 357–366.

Davies, S.W., Turmaine, M., Cozens, B.A., DiFiglia, M., Sharp, A.H., Ross, C.A., Scherzinger, E., Wanker, E.E., Mangiarini, L., and Bates, G.P. (1997). Formation of neuronal intranuclear inclusions (NII) underlies the neurological dysfunction in mice transgenic for the HD mutation. Cell *90*, 537–548.

DiFiglia, M., Sapp, E., Chase, K., Schwarz, C., Meloni, A., Young, C., Martin, E., Vonsattel, J.P., Carraway, R., Reeves, S.A., et al. (1995). Huntingtin is a cytoplasmic protein associated with vesicles in human and rat brain neurons. Neuron *14*, 1075–1081.

DiFiglia, M., Sapp, E., Chase, K.O., Davies, S.W., Bates, G.P., Vonsattel, J.P., and Aronin, N. (1997). Aggregation of huntingtin in neuronal intranuclear inclusions and dystrophic neurites in brain. Science *277*, 1990–1993.

Dingledine, R. (1984). Brain Slices (New York: Plenum Press).

Duff, K., McGuigan, A., Huxley, C., Schulz, F., and Hardy, J. (1994). Insertion of a pathogenic mutation into a yeast artificial chromosome containing the human amyloid precursor protein gene. Gene Ther. *1*, 70–75.

Duyao, M.P., Auerbach, A.B., Ryan, A., Persichetti, F., Barnes, G.T., McNeil, S.M., Ge, P., Vonsattel, J.-P., Gusella, J.F., Joyner, A.L., and MacDonald, M.E. (1995). Inactivation of the mouse Huntington's disease gene homolog *Hdh*. Science *269*, 407–410.

Ferrante, R.J., Kowall, N.W., Beal, M.F., Richardson, E.P., Jr., Bird, E.D., and Martin, J.B. (1985). Selective sparing of a class of striatal neurons in Huntington's disease. Science *230*, 561–563.

Goldberg, Y.P., Nicholson, D.W., Rasper, D.M., Kalchman, M.A., Koide, H.B., Graham, R.K., Bromm, M., Kazemi-Esfarjani, P., Thornberry, N.A., Vaillancourt, J.P., and Hayden, M.R. (1996). Cleavage of huntingtin by apopain, a proapoptotic cysteine protease, is modulated by the polyglutamine tract. Nat. Genet. *13*, 442–449.

Grynkiewicz, G., Poenie, M., and Tsien, R.Y. (1985). A new generation of $Ca2^+$ indicators with greatly improved fluorescence properties. J. Biol. Chem. *260*, 3440–3450.

Gutekunst, C.-A., Levey, A.I., Heilman, C.J., Whaley, W.L., Yi, H.,

Nash, N.R., Rees, H.D., Madden, J.J., and Hersch, S.M. (1995). Identification and localization of huntingtin in brain and human lymphoblastoid cell lines with anti-fusion protein antibodies. Proc. Natl. Acad. Sci. USA *92*, 8710–8714.

Gutekunst, C.-A., Li, S.-H., Yi, H., Mulroy, J.S., Kuemmerle, S., Jones, R., Rye, D., Ferrante, R.J., Hersch, S.M., and Li, X.-J. (1999). Nuclear and neuropil aggregates in Huntington's disease: relationship to neuropathology. J. Neurosci. *19*, 2522–2534.

Hackam, A.S., Singaraja, R., Wellington, C.L., Metzler, M., McCutcheon, K., Zhang, T., Kalchman, M., and Hayden, M.R. (1998). The influence of huntingtin protein size on nuclear localization and cellular toxicity. J. Cell Biol. *141*, 1097–1105.

Hackam, A.S., Singaraja, R., Zhang, T., Gan, L., and Hayden, M.R. (1999). In vitro evidence for both the nucleus and cytoplasm as subcellular sites of pathogenesis in Huntington disease. Hum. Mol. Genet. *8*, 25–33.

Harper, P.S. (1991). Huntington's Disease (Philadelphia: W.B. Saunders).

Hayden, M.R. (1981). Huntington's chorea (Berlin: Springer-Verlag).

Hodgson, J.G., Smith, D.J., McCutcheon, K., Koide, H.B., Nishiyama, K., Dinulos, M.B., Stevens, M.E., Bissada, N., Nasir, J., Kanazawa, K., et al. (1996). Human huntingtin derived from YAC transgenes compensates for loss of murine huntingtin by rescue of the embryonic lethal phenotype. Hum. Mol. Genet. *5*, 1875–1885.

Huntington's Disease Collaborative Research Group (1993). A novel gene containing a trinucleotide repeat that is expanded and unstable on Huntington's disease chromosomes. Cell *72*, 971–983.

Kalchman, M.A., Koide, H.B., McCutcheon, K., Graham, R.K., Nichol, K., Nishiyama, K., Lynn, F.C., Kazemi-Esfarjani, P., Wellington, C.L., Metzler, M., et al. (1997). HIP1, a human homolog of *S. cerevisiae* Sla2p, interacts with membrane-associated huntingtin in the brain. Nat. Genet. *16*, 44–53.

Kim, T.-W., and Tanzi, R.E. (1998). Neuronal intranuclear inclusions in polyglutamine diseases: nuclear weapons or nuclear fallout? Neuron *21*, 657–659.

Klement, I.A., Skinner, P.J., Kaytor, M.D., Yi, H., Hersch, S.M., Clark, H.B., Zoghbi, H.Y., and Orr, H.T. (1998). Ataxin-1 nuclear localization and aggregation: role in polyglutamine-induced disease in *SCA1* transgenic mice. Cell *95*, 41–53.

Li, X.J., Li, S.H., Sharp, A.H., Nucifora, F.C., Jr., Schilling, G., Lanahan, A., Worley, P., Snyder, S.H., and Ross, C.A. (1995). A huntingtin-associated protein enriched in brain with implications for pathology. Nature *378*, 398–402.

Malenka, R.C., Kauer, J.A., Zucker, R.S., and Nicoll, R.A. (1988). Postsynaptic calcium is sufficient for potentiation of hippocampal synaptic transmission. Science *242*, 81–84.

Malenka, R.C., Lancaster, B., and Zucker, R.S. (1992). Temporal limits on the rise in postsynpatic calcium required for the induction of long-term potentiation. Neuron *9*, 121–128.

Mangiarini, L., Sathasivam, K., Seller, M., Cozens, B., Harper, A., Hetherington, C., Lawton, M., Trottier, Y., Lehrach, H., Davies, S.W., and Bates, G.P. (1996). Exon 1 of the *HD* gene with an expanded CAG repeat is sufficient to cause a progressive neurological phenotype in transgenic mice. Cell *87*, 493–506.

Martindale, D., Hackam, A.S., Wieczorek, A., Ellerby, L., Wellington, C.L., McCutcheon, K., Singaraja, R., Kazemi-Esfarjani, P., Devon, R., Bredesen, D.E., Tufaro, F., and Hayden, M.R. (1998). Length of the protein and polyglutamine tract influence localization and frequency of intracellular aggregates of huntingtin. Nat. Genet. *18*, 150–154.

Morris, R.G., Anderson, E., Lynch, G.S., and Baudry, M. (1986). Selective impairment of learning and blockade of long-term potentiation by an N-methyl-D-aspartate receptor antagonist, AP5. Nature *19*, 774–776.

Nasir, J., Floresco, S.B., O'Kusky, J.R., Diewert, V.M., Richman, J.M., Zeisler, J., Borowski, A., Marth, J.D., Phillips, A.G., and Hayden, M.R. (1995). Targeted disruption of the Huntington's disease gene results in embryonic lethality and behavioral and morphological changes in heterozygotes. Cell *81*, 811–823.

Paulson, H.L., Perez, M.K., Trottier, Y., Trojanowski, J.Q., Subramony, S.H., Das, S.S., Vig, P., Mandel, J.-L., Fischbeck, K.H., and Pittman, R.N. (1997). Intranuclear inclusions of expanded polyglutamine protein in spinocerebellar ataxia type 3. Neuron *19*, 333–344.

Reddy, P.H., Williams, M., Charles, V., Garrett, L., Pike-Buchanan, L., Whetsell, W.O., Jr., Miller, G., and Tagle, D.A. (1998). Behavioral abnormalities and selective neuronal loss in HD transgenic mice expressing mutated full-length HD cDNA. Nat. Genet. *20*, 198–202.

Saudou, F., Finkbeiner, S., Devys, D., and Greenberg, M.E. (1998). Huntingtin acts in the nucleus to induce apoptosis but death does not correlate with the formation of intranuclear inclusions. Cell *95*, 55–66.

Schilling, G., Becher, M.W., Sharp, A.H., Jinnah, H.A., Duan, K., Kotzuk, J.A., Slunt, H.H., Ratovitski, T., Cooper, J.K., Jenkins, N.A., et al. (1999). Intranuclear inclusions and neuritic aggregates in transgenic mice expressing a mutant N-terminal fragment of huntingtin. Hum. Mol. Genet. *8*, 397–407.

Skinner, P.J., Koshy, B.T., Cummings, C.J., Klement, I.A., Helin, K., Servadio, A., Zoghbi, H.Y., and Orr, H.T. (1997). Ataxin-1 with an expanded glutamine tract alters nuclear matrix–associated structures. Nature *389*, 971–974.

Spargo, E., Everall, I.P., and Lantos, P.L. (1993). Neuronal loss in the hippocampus in Huntington's disease: a comparison with HIV infection. J. Neurol. Neurosurg. Psychiatry *56*, 487–491.

Vonsattel, J.P., Myers, R.H., Stevens, T.J., Ferrante, R.J., Bird, E.D., and Richardson, E.P., Jr. (1985). Neuropathological classification of Huntington's disease. J. Neuropathol. Exp. Neurol. *44*, 559–577.

Wanker, E.E., Rovira, C., Scherzinger, E., Hasenbank, R., Walter, S., Tait, D., Colicelli, J., and Lehrach, H. (1997). HIP1: A huntingtin interacting protein isolated by the yeast two-hybrid system. Hum. Mol. Genet. *6*, 487–495.

Wellington, C.L., Ellerby, L.M., Hackam, A.S., Margolis, R.L., Trifiro, M.A., Singaraja, R., McCutcheon, K., Salvesen, G.S., Propp, S.S., Bromm, M., et al. (1998). Caspase cleavage of gene products associated with triplet expansion disorders generates truncated fragments containing the polyglutamine tract. J. Biol. Chem. *273*, 9159–9167.

White, J.K., Auerbach, W., Duyao, M.D., Vonsattel, J.P., Gusella, J.F., Joyner, A.L., and MacDonald, M.E. (1997). Huntingtin is required for neurogenesis and is not impaired by the Huntington's disease CAG expansion. Nat. Genet. *17*, 404–410.

Zeitlin, S., Liu, J.-P., Chapman, D.L., Papaioannou, V.E., and Efstratiadis, A. (1995). Increased apoptosis and early embryonic lethality in mice nullizygous for the Huntington's disease gene homologue. Nat. Genet. *11*, 155–162.